Joule

CellPress

Article

Cascade CO_2 electroreduction enables efficient carbonate-free production of ethylene

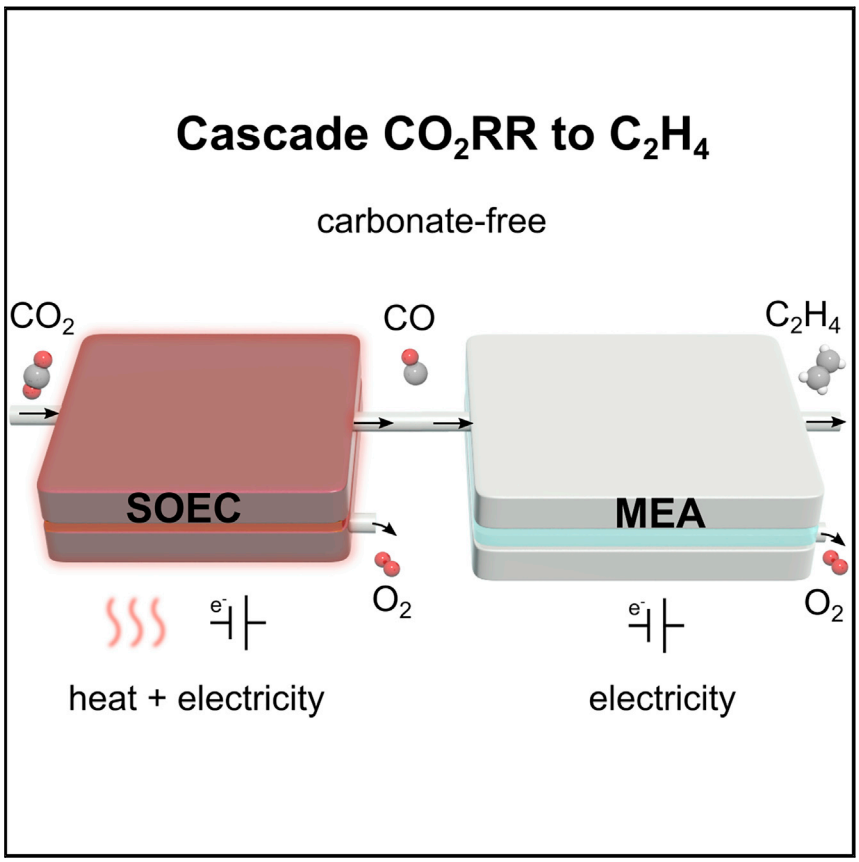

CO_2 electroreduction to chemical feedstocks has suffered from CO_2 reactant loss and a severe energy consumption/production penalty associated with carbonate formation. We divided the process into two cascading steps—CO_2 reduction to CO in a solid-oxide electrolysis cell (SOEC) and CO reduction to multi-carbon products in a membrane electrode assembly (MEA) electrolyser. In the full SOEC-MEA cascade approach, we achieve CO_2-to-C_2H_4 with no loss of CO_2 to carbonate and a ~48% reduction in energy intensity compared with the direct route.

Adnan Ozden, Yuhang Wang, Fengwang Li, ..., Jonas C. Peters, Edward H. Sargent, David Sinton

ted.sargent@utoronto.ca (E.H.S.)
sinton@mie.utoronto.ca (D.S.)

HIGHLIGHTS

Efficient carbonate-free production of ethylene via cascade CO_2 electroreduction

High-rate and efficient ethylene electrosynthesis in membrane electrode assembly

A record-low energy requirement for the electroproduction of ethylene

110 h stable operation at an ethylene energy efficiency of >25%

Ozden et al., Joule 5, 1–14
March 17, 2021
https://doi.org/10.1016/j.joule.2021.01.007

Please cite this article in press as: Ozden et al., Cascade CO_2 electroreduction enables efficient carbonate-free production of ethylene, Joule (2021), https://doi.org/10.1016/j.joule.2021.01.007

Joule

CellPress

Article

Cascade CO_2 electroreduction enables efficient carbonate-free production of ethylene

Adnan Ozden,[1,5] Yuhang Wang,[2,5] Fengwang Li,[2,5] Mingchuan Luo,[2] Jared Sisler,[2] Arnaud Thevenon,[3] Alonso Rosas-Hernández,[3] Thomas Burdyny,[4] Yanwei Lum,[2] Hossein Yadegari,[1] Theodor Agapie,[3] Jonas C. Peters,[3] Edward H. Sargent,[2,*] and David Sinton[1,6,*]

SUMMARY

CO_2 electroreduction provides a route to convert waste emissions into chemicals such as ethylene (C_2H_4). However, the direct transformation of CO_2-to-C_2H_4 suffers from CO_2 loss to carbonate, consuming up to 72% of energy input. A cascade approach—coupling a solid-oxide CO_2-to-CO electrochemical cell (SOEC) with a CO-to-C_2H_4 membrane electrode assembly (MEA)—would eliminate CO_2 loss to carbonate. However, this approach requires a CO-to-C_2H_4 MEA with energy efficiency well beyond demonstrations to date. Focusing on the MEA, we find that an N-tolyl substituted tetrahydro-bipyridine film improves the stabilization of key reaction intermediates, while an SSC ionomer enhances CO transport to the Cu surface, enabling a C_2H_4 faradaic efficiency of 65% at 150 mA cm^{-2} for 110 h. Demonstrating a cascade SOEC-MEA approach, we achieve CO_2-to-C_2H_4 with a ~48% reduction in energy intensity compared with the direct route. We further reduce the energy intensity by coupling CO electroreduction (CORR) with glucose electrooxidation.

INTRODUCTION

The global annual ethylene (C_2H_4) production reached to 185 Mt in 2018, exceeding that of any other organic chemical production.[1] The production of C_2H_4 involves steam cracking of fossil fuel-derived long-chain hydrocarbons—a process that releases 2–3 tons of CO_2 per ton of C_2H_4 produced before the in-plant CO_2 capture.[2] The net process releases ~200 Mt of CO_2 annually,[1] accounting for 0.6% of the total anthropogenic emissions.[3]

CO_2 electroreduction (CO_2RR) using renewable electricity holds promise for low-carbon C_2H_4 production.[4] The present day CO_2RR has reached faradaic efficiencies (FEs) of 70%–80% toward C_2H_4[5–7] and energy efficiencies (EEs) over 30% at current densities over 100 mA cm^{-2}.[5] However, due to the formation of carbonate during CO_2RR (Figure S1), concerns regarding the consequent penalty in energy consumption and production cost have risen.[8,9]

To assess the energy and cost associated with CO_2 reactant loss to carbonate, we performed energy and techno-economic assessments (TEA) for benchmark neutral and alkaline CO_2RR systems from literature, with the ideal and base case scenarios (Notes S1 and S2; Figures S2–S5; Tables S1–S3). Electrolyte regeneration, system operation, and anodic product separation associated with carbonate formation significantly increase energy consumption and cost. The regeneration of alkaline electrolyte induces

Context & scale

CO_2 electroreduction offers a route to net-zero-emission production of C_2H_4—the most-produced organic compound. However, the formation of carbonate in this process causes loss of CO_2 and a severe energy consumption/production penalty. Dividing the CO_2-to-C_2H_4 process into two cascading steps—CO_2 reduction to CO in a solid-oxide electrolysis cell (SOEC) and CO reduction to C_2H_4 in a membrane electrode assembly (MEA) electrolyser—would enable carbonate-free C_2H_4 electroproduction. However, this cascade approach requires CO-to-C_2H_4 with energy efficiency well beyond demonstrations to date. Here, we present a layered catalyst structure composed of a metallic Cu, N-tolyl-tetrahydro-bipyridine, and SSC ionomer that enables efficient CO-to-C_2H_4 in a MEA electrolyser. In the full SOEC-MEA cascade approach, we achieve CO_2-to-C_2H_4 with no loss of CO_2 to carbonate and a total energy requirement of ~138 GJ (ton C_2H_4)$^{-1}$, representing a ~48% reduction in energy intensity compared with the direct route.

Please cite this article in press as: Ozden et al., Cascade CO_2 electroreduction enables efficient carbonate-free production of ethylene, Joule (2021), https://doi.org/10.1016/j.joule.2021.01.007

a penalty of ~278 GJ per ton C_2H_4 produced, accounting for 60%–70% of the total energy requirement (Figures 1A and 1B). Membrane electrode assembly (MEA) electrolysers result in less carbonate formation. However, 6 mol CO_3^- for every mole of C_2H_4 is produced, leading to a 4× increase in membrane resistance,[10] pH-gradient induced high voltages,[11] and 60–90 GJ of additional energy consumption per ton C_2H_4—a process energy penalty of ~35% (Figures 1A and 1B; Tables S1–S3).

Encouraged by recent advances in CO electroreduction,[8,9] we took the view that carbonate-free conversion of CO_2 to C_2H_4 could be realized through two cascading steps (Figure 1C): (A) CO_2 reduction to CO in a high-temperature CO_2-to-CO electrochemical cell (SOEC), which avoids carbonate formation[12] and (B) CO reduction to C_2H_4 (CORR-to-C_2H_4) in an MEA electrolyser (Figure S6). Despite the cascade approach requiring an additional energy input for separation and heating, as well as two separate systems, the cascade route could be competitive with the direct route (employing best-reported metrics in literature as inputs and assuming capital costs fixed to $/kW, Tables S1 and S2). The cascade approach benefits from high process efficiency in the SOEC step, as well as the use of an alkaline electrolyte in the CO-to-C_2H_4 step, without suffering carbonate formation (Tables S1 and S2). For both electroproduction routes, operating potential, FE, and current density are the most important parameters influencing the energy intensity of C_2H_4 production (Figure S7).

RESULTS AND DISCUSSION

CO_2-to-CO conversion in an SOEC

We first established the performance of CO_2-to-CO in an SOEC. The SOEC was operated at 800°C. We achieved a 95% CO FE and an 89% CO EE at 815 mA cm^{-2} and at a CO_2 flow rate of 20 sccm (Figure 2A). This is equal to a CO_2-to-CO single-pass efficiency of ~36%. Utilization can be further improved by lowering flow rates or increasing current to the limit imposed by the CO disproportionation reaction, also referred to as the Boudouard reaction.[13,14] Here, a maximum CO_2-to-CO single-pass efficiency of ~55% was obtained (Figure 2B) at a CO FE of ~77% and current density of 1.25 A cm^{-2}. At lower flow rates, considering both CO selectivity and CO_2 single-pass conversion, the current density versus CO_2 flow rate ratio of 815:15 (mA cm^{-2}:sccm) was confirmed to be the best condition under which we observed a constant CO FE of ~91% and CO_2-to-CO single-pass conversion of ~45% (Figure 2C). The energy input requirement for this SOEC step was 13.49 GJ/ton CO.

CORR MEA for C_2H_4 electroproduction

For C_2H_4 production, our analysis shows that the success of this two-step approach relies on CO-to-C_2H_4 in an MEA electrolyser (Figures S3–S5). A high C_2H_4 FE (> 60%) is required in concert with a high current density (>150 mA cm^{-2}) and low operating full-cell potential (< 3 V). To date, the highest FE for CO-to-C_2H_4 in MEA electrolysers remains below 40%, and the corresponding C_2H_4 partial current density (j_{C2H4}) is less than 60 mA cm^{-2}.[8] We therefore sought to develop a high-performance CO-to-C_2H_4 MEA electrolyser that is essential for efficient, cascade CO_2-to-C_2H_4 conversion.

We first electrodeposited copper (Cu) catalysts under CO_2-rich conditions as MEA cathodes. A CO_2-rich environment increases Cu(100) exposure,[15] which enhances the selectivity toward C_2H_4 in CO_2RR.[8,16] However, a simple Cu surface has large regions that do not have ready access to CO on the hydrophilic surface (Figure S8).[17] We assembled the MEA—using electrodeposited Cu as the cathode electrode, anion exchange membrane as the solid-state electrolyte, and iridium oxide supported on a titanium mesh as the anode electrode—and investigated the CORR performance. This catalyst consequently favors H_2 production, allowing C_2H_4

[1]Department of Mechanical and Industrial Engineering, University of Toronto, 5 King's College Road, Toronto, ON M5S 3G8, Canada

[2]Department of Electrical and Computer Engineering, University of Toronto, 10 King's College Road, Toronto, ON M5S 3G4, Canada

[3]Joint Center for Artificial Photosynthesis and Division of Chemistry and Chemical Engineering, California Institute of Technology, Pasadena, CA 91125, USA

[4]Department of Chemical Engineering, Delft University of Technology, Van der Maasweg 9 2629 HZ Delft, the Netherlands

[5]These authors contributed equally

[6]Lead contact

*Correspondence: ted.sargent@utoronto.ca (E.H.S.), sinton@mie.utoronto.ca (D.S.)

https://doi.org/10.1016/j.joule.2021.01.007

Please cite this article in press as: Ozden et al., Cascade CO_2 electroreduction enables efficient carbonate-free production of ethylene, Joule (2021), https://doi.org/10.1016/j.joule.2021.01.007

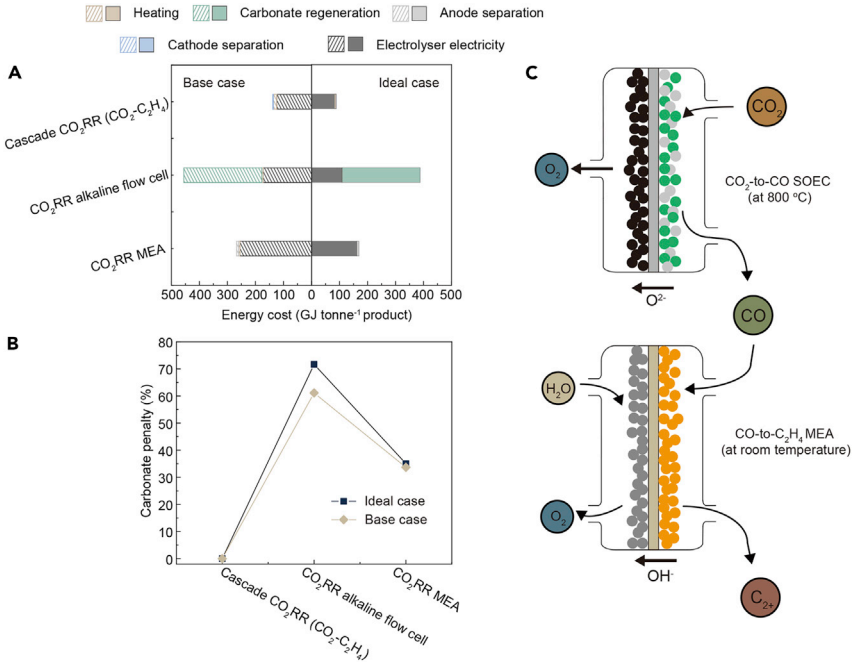

Figure 1. Carbonate-formation-free CO_2-to-C_2H_4 production through cascade CO_2RR

(A) Comparison of energy consumption for C_2H_4 production in various systems.

(B) The carbonate penalty (i.e., the fraction of energy consumption due to carbonate formation) in the various systems. TEA calculation details are provided in the Supplemental information.

(C) A schematic illustration of renewable CO_2-synthesized C_2H_4 in a combined system consisting of a CO_2-to-CO SOEC and a CO-to-C_2H_4 MEA.

production with a maximum FE of only 50% at a low partial current density (j_{C2H4}) of 60 mA cm^{-2} (Figure S8).

Modifying the Cu surface with hydrophobic aliphatic molecules or ionomers has been demonstrated to increase reactant availability at the catalytic interface[17–19] and improve the selectivity and activity toward C_2H_4 electroproduction.[20] We therefore added a $(C_4HF_7O_4S.C_2F_4)_x$ short-side-chain (SSC) ionomer coating on the Cu surface.[21] We found that H_2 selectivity was suppressed by 10%–30% across the screened cell potential window, and that the highest j_{C2H4} increased to ~155 mA cm^{-2} (Figure S9). However, the maximum C_2H_4 FE remained at ~50%.

The strategy we pursued to promote C_2H_4 at lower potentials was to alter the adsorption of the key CO* intermediate via a molecular tuning strategy.[6] We therefore introduced an *N-tolyl substituted tetrahydro-bipyridine* (labeled Py) interlayer between Cu and SSC by an electro-dimerization method.[6] This metal:molecular film:ionomer combination (labeled Cu:Py:SSC), in which SSC improves the CO diffusion at the outer layer and Py provides more atop-bound CO* on the Cu surface (Figure 3A), enabled the highest C_2H_4 FE of 65% $\pm$ 1% at a 2.5 V full-cell potential, and provided a j_{C2H4} of 130 mA cm^{-2} at 2.6 V (Figure 3B). A detailed CORR-to-C_2H_4 performance of the Cu:Py:SSC, Cu:SSC, and bare Cu is summarized in Tables S4–S6. To gain an insight into the enhanced CO-to-C_2H_4 selectivity and productivity, we investigated the catalysts using scanning and transmission electron microscopy (SEM and TEM, respectively). We observed a dendritic Cu fully covered by the Py molecule and SSC ionomer (Figures 3C and S10). The Cu catalyst had high crystallinity, confirmed

Please cite this article in press as: Ozden et al., Cascade CO_2 electroreduction enables efficient carbonate-free production of ethylene, Joule (2021), https://doi.org/10.1016/j.joule.2021.01.007

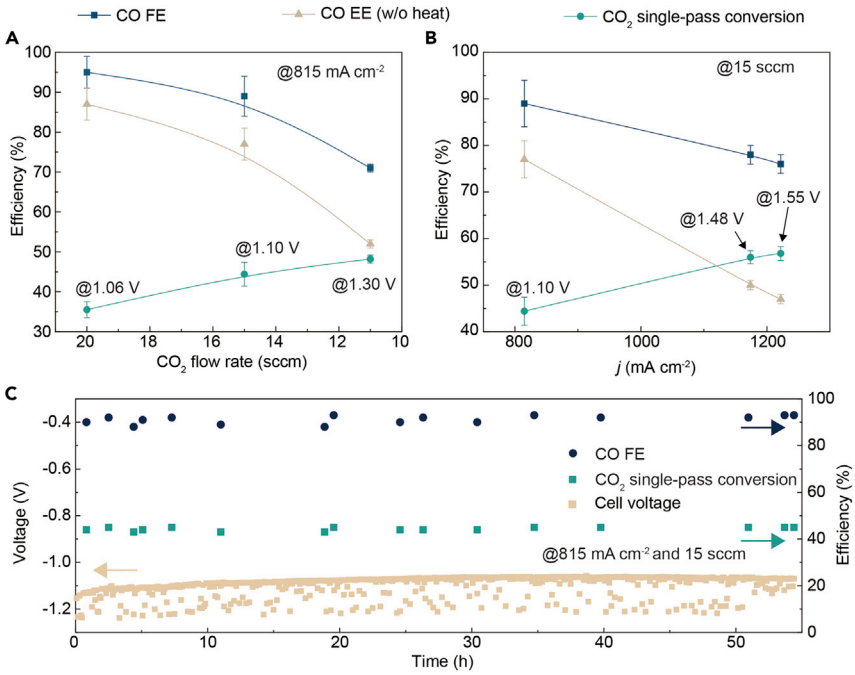

Figure 2. CO_2-to-CO conversion in an SOEC

(A) CO_2-to-CO Faradaic efficiency, single-pass conversion, and energy efficiency in a commercial 2.5-cm NiO-YSZ/YSZ/GDC/LSC at various CO_2 flow rates. (B) CO_2-to-CO Faradaic efficiency, single-pass conversion, and energy efficiency in a commercial 2.5-cm NiO-YSZ/YSZ/GDC/LSC at various current densities. The increase in the CO_2 single-pass conversion by lowering CO_2 flow rates or increasing current density was caused by the CO disproportionation reaction, which is also known as the Boudouard reaction.

(C) The CO_2-to-CO Faradaic efficiency, single-pass conversion, and cell voltage profiles during the 55-h test at 815 mA cm^{-2} and a CO_2 flow rate of 15 sccm. The operating temperature is 800°C. The error bars correspond to the standard deviation of three independent measurements.

by the grazing-incidence wide-angle X-ray scattering (GIWAXS) (Figure S11). We conclude that there was full coverage of Py and SSC on the Cu surface.

We then conducted *in situ* Raman spectroscopic studies on the catalytic interface.[22–25] We observed a stabilized atop-bound CO*,[6] known to favor the key CO–CO dimerization step,[16,26,27] evidenced by the transformation of CO* adsorption configurations (Figure S12): the fraction of the area of atop-bound CO* at the wave number of ~2,080 cm^{-1}[28] increased to 33% when Py molecule was electrodeposited onto the Cu surface. By contrast, bridge-bound CO* at 1,980–2,020 cm^{-1}[28–30] dominated the adsorption configurations on the bare Cu.

We then sought to optimize the full-cell EE by increasing the alkalinity of the anolyte (Figure 3D; Tables S7–S9). With increasing KOH concentrations, the C_2H_4 FE peak increased to ~65% (Figure 3D), an example of alkalinity favoring C_{2+} production.[5,31,32] The ionic conductivity was also improved by high alkalinity, and the j_{C2H4} at each C_2H_4 FE peak increased from ~47 to ~100 mA cm^{-2}, and the full-cell potential reduced from 2.8 to 2.5 V in the range of 0.1 to 3 M KOH (Figures 3D and S13; Tables S6–S8). However, 5 M KOH lowered the j_{C2H4} to 81 mA cm^{-2} at all applied potentials (Figure S14; Table S9), which we attribute to a low CO concentration at the catalyst layer under this condition (Figure S15). Considering C_2H_4 FE, j_{C2H4}, and full-cell potential, the 3 M KOH is the best anolyte for CO-to-C_2H_4 conversion in this system.

Please cite this article in press as: Ozden et al., Cascade CO_2 electroreduction enables efficient carbonate-free production of ethylene, Joule (2021), https://doi.org/10.1016/j.joule.2021.01.007

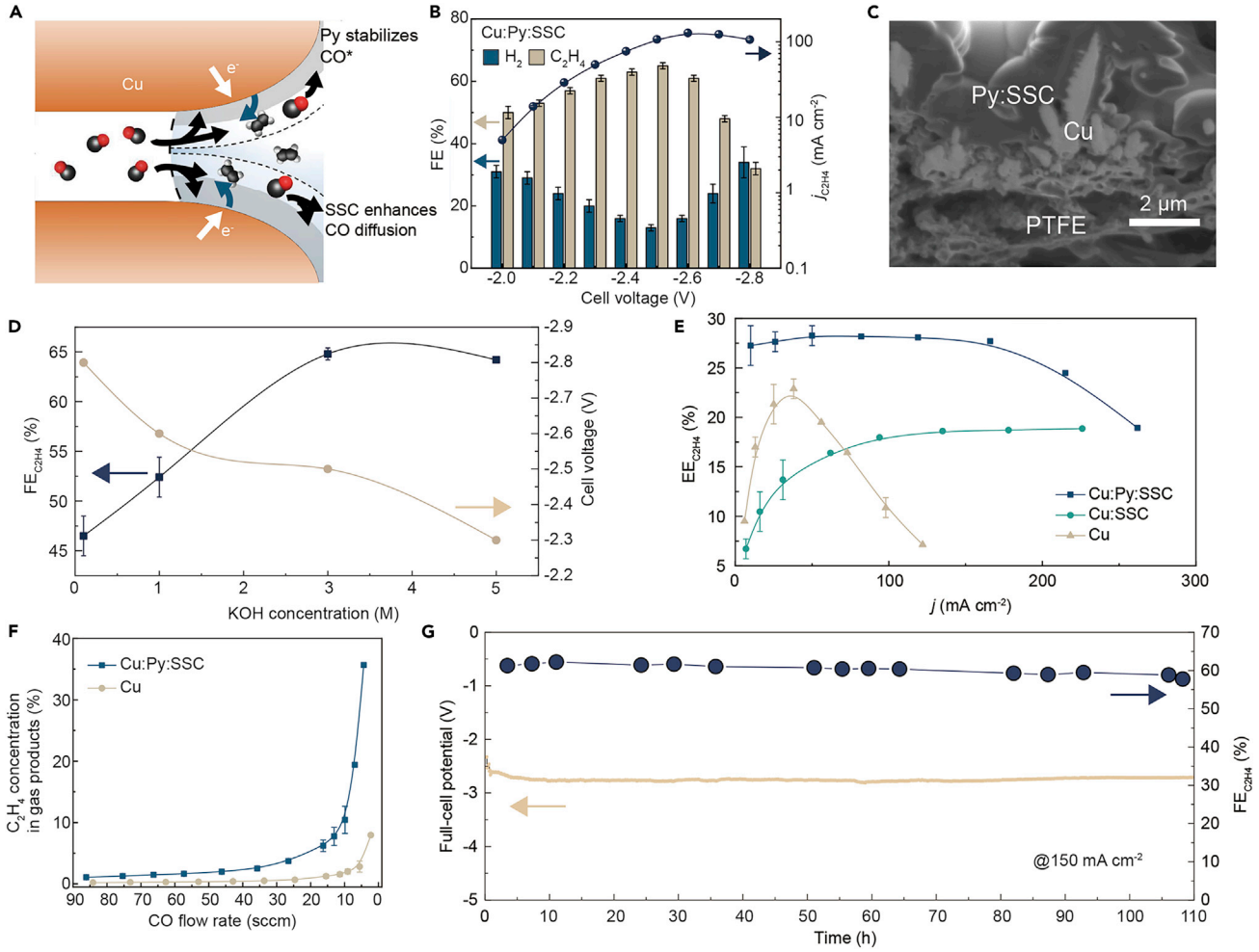

Figure 3. CO-to-C_2H_4 electroreduction in an MEA

(A and B) Introducing additives to improve CO diffusion and stabilize CO* intermediates leads to enhanced C_2H_4 selectivity and activity.

(C) Cross-sectional SEM images of the Cu:Py:SSC catalyst. The scale bar is 2 μm.

(D) The C_2H_4 FE and full-cell voltages in different anolytes.

(E) Comparison of the CO-to-C_2H_4 EEs obtained using the Cu:Py:SSC catalyst and controls in MEAs with 3 M KOH. (F) Comparison of the C_2H_4 concentrations obtained using the Cu:Py:SSC catalyst and Cu control in MEAs with 3 M KOH.

(G) C_2H_4 FE and full-cell voltage of the MEA equipped with a Cu:Py:SSC cathode for 110 h at 150 mA cm^{-2}. The error bars correspond to the standard deviation of three independent measurements.

Further comparisons in 3 M KOH revealed that the Cu:Py:SSC combination outperformed the Cu:SSC and bare Cu in terms of both j_{C2H4} and C_2H_4 full-cell EE (Figure 3E). Importantly, we achieved—when compared with bare Cu—a 5× increase in the peak j_{C2H4} (from 26 ± 2 to 129 ± 1 mA cm^{-2}) and a 1.4× increase in the peak full-cell EE (from 21% ± 2% to 29% ± 1%) using the Cu:Py:SSC combination (Tables S4 and S6). We observed typical CORR gas and liquid products in the current density range of 25 to 250 mA cm^{-2}, with the peak C_{2+} FE of ~85% at 160 mA cm^{-2} (Table S10; Figure S16). A stable 28% C_2H_4 full-cell EE for the Cu:Py:SSC system was achieved in the current density range of 80 to 170 mA cm^{-2}, whereas the Cu:SSC and bare Cu systems were limited to EEs of <20% in this current density range (Figure 3E). Further optimization of the CO coverage on the Cu:Py:SSC catalyst—through co-feeding CO with N_2—improved the C_2H_4 full-cell EE to 30% ± 1% at a constant current density of 100 mA cm^{-2} (Table S11).

Please cite this article in press as: Ozden et al., Cascade CO_2 electroreduction enables efficient carbonate-free production of ethylene, Joule (2021), https://doi.org/10.1016/j.joule.2021.01.007

We investigated the C_2H_4 production rate (R_{C2H4}) and its concentration in the product stream. The Cu:Py:SSC combination produced C_2H_4 at almost 0.68 mmol cm^{-2} h^{-1} and 1.5 and 6 times faster than the Cu:SSC and bare Cu, respectively (Figure S17). Using an inlet CO flow rate of 4 sccm, we obtained a ~36% C_2H_4 concentration in gas products (Figure 3F; Table S12). This translated to a ~26% CO-to-C_2H_4 single-pass conversion and is ~3 times higher than that of bare Cu.

We confirmed the stability of the MEA with the Cu:Py:SSC catalyst using 3 M KOH at 150 mA cm^{-2}. The system maintained a constant C_2H_4 FE of 61% $\pm$ 2% and a full-cell potential of 2.73 $\pm$ 0.02 V for 110 h with no performance degradation (Figure 3G). We analyzed the cathode electrode after 110-h continuous electrolysis using electron microscopy, X-ray photon spectroscopy, and soft X-ray adsorption spectra (sXAS) at the N K-edge. The Cu morphology and Py:SSC coating as well as associated features were retained (Figures S18–S20). The MEA equipped with the Cu:Py:SSC catalyst—when taking the carbonate formation penalty into account—outperformed literature benchmarks,[6,8,11,33–35] including both CO_2RR and CORR, in C_2H_4 FE, j_{C2H4}, C_2H_4 full-cell EE and operation duration (Table S13).

Cascade CO_2-to-C_2H_4 electroreduction in the integrated system

We built an integrated system for carbonate-free CO_2-to-C_2H_4 electroproduction (Figure 1C) by combining the high-performance CO-to-C_2H_4 MEA with the CO_2-to-CO SOEC. The SOEC was operated at 800°C and a current density of 550 mA cm^{-2}, yielding a ~95% CO FE, ~86% CO full-cell EE (for electricity only), and ~48% single-pass utilization (Figure S21). The inlet CO_2 flow rate was set at 10 sccm to ensure the optimal 815:15 (mA cm^{-2} versus sccm) ratio of current density: CO_2 flow rate and an outlet CO production of ~4.5 sccm for a high CO-to-C_2H_4 single-pass conversion utilization. The products of the SOEC were purified using CO_2 capture solution containing 30% ethanolamine before feeding into the CO-to-C_2H_4 MEA. The temperature of the purified gas supplied to the MEA electrolyser was measured to be 25°C. The system had a peak CO_2-to-C_2H_4 EE (for electricity only) of 20% (Figure 4A) and a maximum single-pass conversion of ~11% for CO_2-to-C_2H_4 with no loss of CO_2 to carbonate formation in electrolytes (Figure 4B). The combined system produced C_2H_4 at a peak rate of 1.3 mmol h^{-1} at 120 mA cm^{-2} (Figure 4C), along with a C_{2+} FE of ~76% (Table S14). The system maintained the peak single-pass conversion and productivity in CO_2-to-C_2H_4 at 120 mA cm^{-2} for 40 h of uninterrupted operation (Figure 4D). The full cascade system achieved a carbonate-free electroproduction of C_2H_4 with an energy intensity of 138 GJ (ton C_2H_4) $^{-1}$, a major savings relative to the direct route (~267 GJ (ton C_2H_4) $^{-1}$).

Having established the system performance in a side-by-side comparison with previous on-step CO_2R processes, we took the MEA in the cascade system a step further. We replaced the oxygen evolution reaction (OER) with the glucose electrooxidation reaction (GOR) for which the thermodynamic potential is ~1 V less than that of OER.[36] We detected gluconate, glucuronate, glucarate, and formate—all products with values higher than that of glucose—as the major GOR products in the current density range of 40 to 200 mA cm^{-2} (Table S15; Figure S22). We found that coupling the CORR and GOR in alkaline media reduces the potential requirement approximately by 1 V at industrially relevant current densities (Figures 4E and S23; Tables S16–S19). At a current density of 120 mA cm^{-2}, we obtained a C_2H_4 FE of ~55% and a C_{2+} FE of ~90% at an MEA full-cell potential of 1.27 V (Figure 4E; Tables S18 and S20). This voltage reduction enables a total energy requirement of ~89 GJ (ton C_2H_4) $^{-1}$, which represents a 35% reduction in the energy consumption compared with the MEA cell using OER anode at the same current density

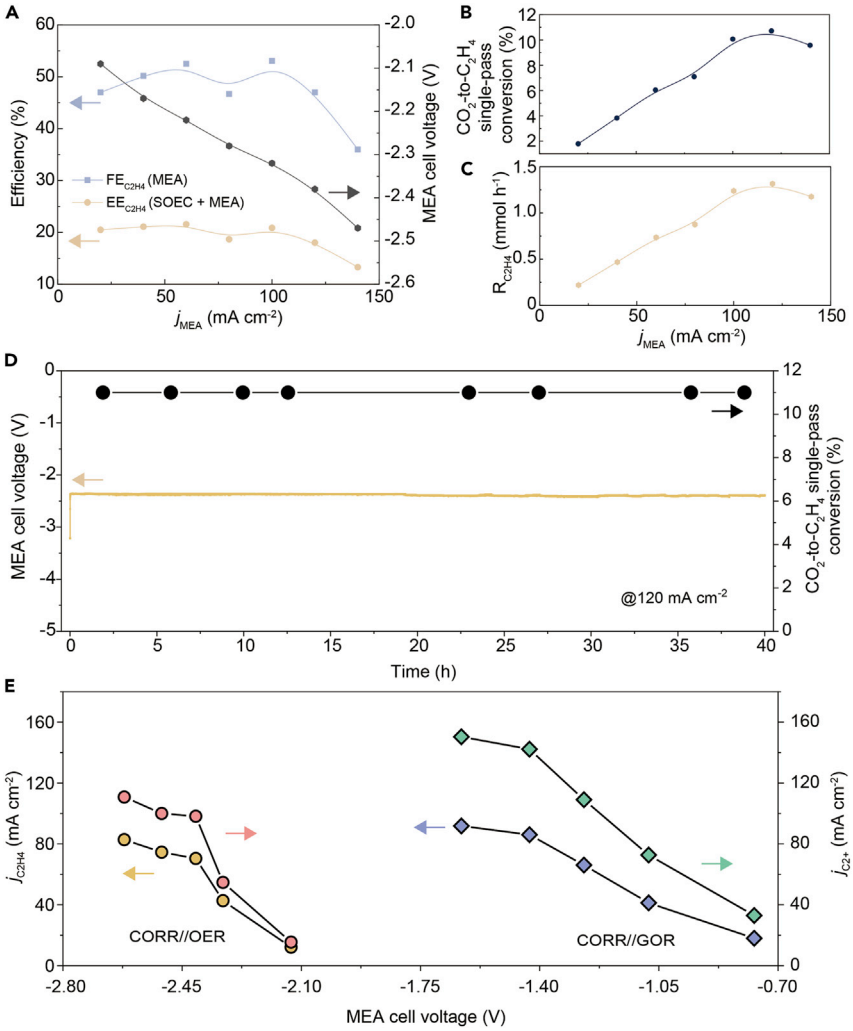

Figure 4. C_2H_4 production performance in the cascade CO_2RR

(A) The C_2H_4 FE and cell voltage of the CO-to-C_2H_4 MEA in the cascade CO_2RR, and the C_2H_4 EE of the cascade CO_2RR.

(B) CO_2-to-C_2H_4 single-pass conversion of the cascade CO_2RR at different operating current densities for the CO-to-C_2H_4 MEA. (C) C_2H_4 production rates of the cascade CO_2RR at different operating current densities for the CO-to-C_2H_4 MEA.

(D) Extended CO_2-to-C_2H_4 single-pass conversion performance of the MEA in the cascade CO_2RR.

(E) Effect of anodic reaction on the CORR performance metrics of the MEA in the cascade CO_2RR.

(~138 GJ (ton C_2H_4)$^{-1}$) (Table S21). All earlier comparisons involve OER only, both in the cascade system and in all reference cases. This additional GOR result highlights the potential to reduce the energy intensity of C_2H_4 production further. Here, we also note that although the anodic products—gluconate, glucuronate, glucarate, and formate—are more valuable than the glucose input, making a full economic case for the anode-side upgrading would require a detailed assessment of multiple separations, which is beyond the scope of this work.

Despite the gains demonstrated here, profitable C_2H_4 electroreduction with cascade CO_2RR will require further improvements in performance metrics, including selectivity, current density, single-pass utilization, and energy efficiency—in both the first step (CO_2-to-CO in SOEC) and second step (CO-to-C_2H_4 in MEA) (Note

S3; Table S21). Further reductions in the capital and operational costs of both systems will also bring the C_2H_4 electroproduction closer to viability (Note S3; Table S21).

Conclusions

We developed a cascade approach to CO_2-to-C_2H_4 conversion that avoids the formation of carbonate and the associated energy penalties, combining an SOEC with a high-performance CORR MEA system designed here. We designed a layered catalyst structure composed of a metallic Cu, N-tolyl-tetrahydro-bipyridine, and SSC ionomer to achieve a high-rate and efficient CO-to-C_2H_4 conversion in a MEA electrolyser. The combined functions of each layer raised the device C_2H_4 FE to 65%, at a full-cell C_2H_4 EE of 28% across a broad range of current densities, versus the <50% FEs of the bare and single-layer catalyst structures. To drive an end-to-end CO_2 conversion process without the loss of CO_2 to carbonate, we paired our MEA electrolyser with a SOEC for CO_2-to-CO conversion. With the CO stream produced from the SOEC, the MEA system generated C_2H_4 at a peak rate of 1.3 mmol h^{-1} and maintained continuous operation for 40 h. The full cascade system required ~138 GJ (ton C_2H_4) $^{-1}$, achieving significant savings over the directly comparable one-step CO_2-to-C_2H_4 route (~267 GJ (ton C_2H_4) $^{-1}$). Having established the direct comparison with existing systems on the basis of OER anode reactions in all cases, we devised an approach to reduce the energy consumption of the MEA further, switching the OER anode to GOR. With this enhancement, the cascade SOEC-MEA system requires a total energy requirement of ~89 GJ (ton C_2H_4) $^{-1}$. These results demonstrate the potential to electrocatalytically convert CO_2 to C_2H_4 without carbonate production and the associated energy penalties. The result is a record-low energy requirement for the production of the world's most-produced organic compound.

EXPERIMENTAL PROCEDURES

Resource availability

Lead contact

Further information and requests for resources and materials should be directed to and will be fulfilled by the lead contact, David Sinton (sinton@mie.utoronto.ca).

Materials availability

This study did not generate new unique materials.

Data and code availability

The data presented in this work are available from the corresponding authors upon reasonable request.

Materials

All solvents and reagents, unless otherwise stated, were obtained from commercial sources (Sigma-Aldrich and Merck) and used without further purification. D_2O (D 99.5%), d-chloroform (D 99.8%), and d_6-DMSO (D 99.8%) were purchased from the Cambridge Isotope Laboratories.

Molecule synthesis

The tolylpyridinium triflate additive was synthesized according to previous report.[22,37] Before usage, the additive was recrystallized two times from a mixture of MeOH:ether (1:5) and metal traces impurities were removed using activated Chelex resin.[38]

Please cite this article in press as: Ozden et al., Cascade CO_2 electroreduction enables efficient carbonate-free production of ethylene, Joule (2021), https://doi.org/10.1016/j.joule.2021.01.007

Electrode preparation

The gas-diffusion electrode (GDE) developed was composed of two catalyst layers: the sputtered Cu layer and the electrodeposited Cu layer. We first magnetically sputtered a 150-nm Cu seed onto the polytetrafluoroethylene (PTFE) substrate with a mean pore size of 450 μm and a sputtering rate of 0.50 Å s^{-1} under 10^{-6} Torr. We then electrodeposited the Cu catalyst onto the 15-nm Cu-sputtered PTFE substrate. The solution prepared for the electrodeposition was composed of 0.1 M copper bromide (98%, Sigma-Aldrich), 0.2 M sodium tartrate dibasic dehydrate (purum p.a., ≥98.0% [NT]), and 1.0 M potassium hydroxide (KOH, Sigma-Aldrich). We performed the electrodeposition at −400 mA cm^{-2} for 90 s under the continuous flow of CO_2. We carried out the electrodeposition in a flow electrolyser composed of anode and cathode flow compartments, separated by an anion exchange membrane (AEM, Sustainion X37–50 grade 60, Dioxide Materials). During the electrodeposition, pure CO_2 with the constant flow rate of 80 standard cubic centimeters per minute (sccm) was supplied to the cathode compartment while 1 M KOH was being circulated through the anode compartment. A nickel foam with a geometric area of 9 cm^2 and an Ag/AgCl (3 M KCl) were used as the counter electrode and reference electrode, respectively.

N-arylpyridinium-derived film deposition

The surface of the Cu catalyst was modified by electrodepositing a 10–20 nm-thick *N-tolyl-tetradihydro-bipyridine* (Py) film from a solution containing 0.1 M $KHCO_3$ and 10 mM *N-tolyl-pyridinium triflate* precursor. The electrodeposition was performed in a three-electrode configuration, in which Ag/AgCl (3 M KCl) was the reference electrode, the electrodeposited Cu was the working electrode, and platinum (Pt) foil was the counter electrode. The electrodeposition was performed via a cyclic voltammetry method in a potential range of −0.6 and −2.0 V, with a scanning rate of 50 mV s^{-1}.

SSC ionomer deposition

The Py-molecule-coated Cu catalysts were then modified by spray deposition of 10–15 nm-thick ionomer layer with a solution containing 16.88 μl cation exchange perfluorosulfonic acid (PFSA) ionomer with SSC (Aquivion D79-25BS) and 3 mL methanol (99.8%, anhydrous, Sigma-Aldrich). Prior to the spray deposition, the solution of SSC ionomer and methanol was sonicated for 1 h to ensure homogeneous dispersion of polymeric binder in the solvent. The resulting electrode was then dried overnight under room conditions prior to performance testing.

Materials characterization

SEM imaging and energy dispersive X-ray (EDX) elemental mapping of the electrodes were carried out using a high-resolution scanning electron microscope (HR-SEM, Hitachi S-5200). X-ray photoelectron spectroscopy (XPS) measurements were performed in electron spectroscopy for chemical analysis (ESCAC) system (PHI 5700), equipped with Al Kα X-ray energy source (1,486.6 eV). Transmission electron microscopy (TEM) images were collected by using a field emission transmission electrode microscope (Hitachi HF3300). GIWAXS measurements were performed at beamline Spring-8 BL-12B2 of the National Synchrotron Radiation Center (NSRRC). X-ray adsorption spectroscopy (XAS) measurements were performed at the high-resolution spherical grating monochromator (SGM) 11ID-1 beamline of the Canadian Light Source. Athena and Artemis software incorporated into standard IFEFFIT package was employed to process the XAS data.

Please cite this article in press as: Ozden et al., Cascade CO_2 electroreduction enables efficient carbonate-free production of ethylene, Joule (2021), https://doi.org/10.1016/j.joule.2021.01.007

In situ Raman measurements

In situ Raman measurements were carried out via inVia Raman Microscope equipped with a water immersion objective (63x, Leica Microsystems), a 785 nm laser, and a modified flow electrolyser with an Ag/AgCl (3 M KCl) reference electrode and a platinum (Pt) counter electrode. Raman signals were processed with certain considerations. The ratio of atop *CO and bridge *CO was calculated by the integration of the corresponding Raman intensity within one spectrum. Only atop/bridge ratios (equivalent to intensities relative to a reference), instead of absolute intensities, were compared for different samples. Further, to ensure the quality of the Raman spectroscopic signal, in the measurements, we averaged 10 scans per spectrum and smoothed and baseline corrected all spectra using the Renishaw WiRE (version 4.4) software. The assignment of the Raman shift is based on cross-referenced literature[23,25,39] and on our prior study of a library of Py-based molecules for CO_2 conversion.[6]

Electrocatalytic measurement of CO-to-C_2H_4 conversion

The electrocatalytic measurements of CO-C_2H_4 conversion were performed in a MEA electrolyser (Dioxide Materials, 5 cm^2 geometric active surface area). Cu:Py:SSC electrodes were used as the cathodes.

To fabricate the Ti-IrO_2 anode electrodes for OER, commercially available titanium (Ti) meshes (Fuel Cell Store) were first etched in a boiling solution of 6 M HCl for 30 min. The etched Ti screens were then immersed into a solution composed of iridium (IV) oxide dehydrate (Premion, 99.99% metals basis, Ir 73 min, Alfa Easer), isopropanol (Sigma-Aldrich), and HCl (ACS reagent, 37%, Sigma-Aldrich), and were sequentially dried and sintered. The last two steps of the procedure were repeated until the total Ir loading of 2 mg cm^{-2} was achieved. AEM membranes (4 × 4 cm^2, Sustainion X37–50 grade 60, Dioxide Materials) were used in all the performance experiments. The AEM membranes were activated in 1 M KOH solution for at least 24 h before testing.

To fabricate the Pt–C anode electrodes for GOR, commercially available platinum on graphitized carbon powder (Sigma-Aldrich, Pt-C, 40 wt % Pt on Vulcan XC72) was first physically mixed with SSC ionomer (Aquivion D79-25BS) in a glass beaker and then sonicated for 1 h. The resulting catalyst ink was then spray coated on both sides of the hydrophilic carbon cloth until the Pt loading of 0.5 mg cm^{-2} achieved.

During the performance testing, KOH solutions (for OER) or KOH + glucose solutions (for GOR) were supplied to the anode flow field with a flow rate of 10 mL min^{-1}, and humidified CO was fed into the cathode flow field with the constant flow rate of 80 sccm. The reaction was initiated by applying a negative potential. The voltage increments were made with sufficiently small increments upon completion of at least 15 min stable operation. The gas products were analyzed by injecting the gas samples collected in 1 mL volumes via gas-tight syringes (Hamilton) in a gas chromatograph (GC, PerkinElmer Clarus 580) equipped with a flame ionization detector (FID) and a thermal conductivity detector (TCD).

For the extended CORR operations, the MEA electrolyser was operated at constant current densities of 150 mA cm^{-2} (for MEA only) and 120 mA cm^{-2} (for cascade SOEC-MEA system). For the extended CORR operation, AEM membranes (4 × 4 cm^2, Fumasep FAA-3-50, FuMA-Tech) were used due to their high stability under alkaline conditions. The AEM membranes were activated in 3 M KOH solution at 25°C for at least 48 h before testing. The gas products were collected at frequent time intervals, and for each data point, three independent injections were made,

and thus each selectivity point presented was calculated by averaging the FE values obtained from three consecutive injections.

CO_2-to-C_2H_4 measurements in the cascade SOEC-MEA system

An open flanges solid-oxide electrolysis cell (SOEC) setup (Fiaxell SOFC Technologies, Switzerland), equipped with a 25 mm electrode-supported cell (Fuel cell materials, USA), was used to convert CO_2 into CO. The cell possessed a geometric active area of 1.2 cm^2. The SOEC setup was operated at 800°C and 815 mA cm^{-2} with a CO_2 inlet flow rate of 15 sccm. The outlet of the SOEC setup was connected to a CO_2 capture solution containing 30 wt % aqueous ethanolamine solution. The purified CO at 25°C was then supplied to the MEA electrolyser for C_2H_4 electroproduction from CO. In the MEA electrolyser, 3 M KOH was used as the anolyte, and the CO-to-ethylene conversion was performed at current densities in the range of 20 and 200 mA cm^{-2}.

Faradaic efficiency and energetic efficiency calculations

FE toward any gas product was calculated using the following equation:

$$\text{Faradaic Efficiency} = \frac{Fn_aV_{gas}c_a}{i_{overall}V_m} \qquad \text{(Equation 1)}$$

where F stands for the Faraday constant, n_a stands for the number of electron transfer needed for the production of 1 mol of product α, V_{gas} stands for the flow rate of supplied gas, c_a stands for the detected concentration of product α via GC (ppm), $i_{overall}$ stands for the overall current measured, and V_m stands for the unit molar volume of supplied gas.

The full-cell EE of the MEA electrolyser toward ethylene production was calculated using the expression given below:

$$EE = \frac{E_{C_2H_4-thermo}FE_{C_2H_4}}{E_{full-cell}} \qquad \text{(Equation 2)}$$

where $E_{C2H4-thermo}$ represents the thermodynamic cell potential for C_2H_4 (−1.06 V for CO-to-C_2H_4), FE_{C2H4} represents the FE toward C_2H_4, and $E_{full-cell}$ represents the full-cell voltage applied.

Liquid products of CORR and GOR were analyzed by nuclear magnetic resonance spectrometer Agilent DD2 600 MHz) by using dimethylsulfoxide as an internal standard.

CO diffusion modeling

The concentration of CO in the electrolyte and that present at the catalyst's surface was determined using a 1D reaction-diffusion model. The model is adapted from a previous report,[5] which modeled the diffusion of CO_2 across a gas-diffusion layer for various electrolytes, current densities, and pressures. Unlike the CO_2 model, CO diffusion into the electrolyte at 0 mA cm^{-2} does not directly affect the local pH or change the concentration of CO or OH^- as a function of distance into the electrolyte. The governing equations for the simulation are shown below and extend from the gas-liquid interface of the gas-diffusion layer at x = 0 μm to an assumed diffusion layer boundary thickness of x = 500 μm into the electrolyte.

$$\frac{\partial[CO]}{\partial t} = D_{CO}\frac{\partial^2[CO]}{\partial x^2} - R_{CO} \qquad \text{(Equation 3)}$$

$$\frac{\partial[OH^-]}{\partial t} = D_{OH^-}\frac{\partial^2[OH^-]}{\partial x^2} + R_{OH} \quad \text{(Equation 4)}$$

where RCO and ROH account for the consumption of CO in the reduction reaction and the production of OH^-, respectively. These reactions are assumed to occur homogeneously throughout the catalyst layer such that the source and sink of CO and OH^- are spatially dependent:

$$R_{CO} = \frac{j}{F}\left(\frac{FE_{ethlyene+enthanol}}{n_{ethylene}} + \frac{FE_{acetate}}{n_{acetate}} + \frac{FE_{n-propanol}}{n_{n-propanol}}\right)\frac{1}{\varepsilon L_{catalyst}}, 0 \le x \le L_{catalyst} \quad \text{(Equation 5)}$$

$$R_{OH} = \frac{j}{F}\frac{1}{\varepsilon L_{catalyst}}, 0 \le x \le L_{catalyst} \quad \text{(Equation 6)}$$

where *F* is Faraday's constant and taken as 96,485 C mol^{-1} and *j* is the geometric current density. As was done previously, a catalyst layer porosity, ε, of 60% was assumed. Based upon the experimental results, product selectivities of 15% hydrogen, 50% ethylene + ethanol, 10% acetate, and 25% n-propanol are assumed for all simulations to approximately account for the number of electrons transferred per CO molecule consumed. A reaction thickness of 100 nm was assumed for the catalyst layer ($L_{catalyst}$ = 100 nm). The maximum solubility of CO in the electrolyte was modeled using Henry's constant at 1 atm and 298 K as well as taking salting-out effects into account via the Sechenov equation.

A no-flux boundary condition was imposed at the left-hand boundary for OH^- while the concentration of CO was initially described by the solubility of CO in the imposed KOH concentration and partial pressure conditions. Both CO and KOH were fixed to their bulk electrolyte concentrations at the boundary layer thickness of 500 μm. The concentration profiles of CO and OH^- were then found at steady state for a variety of KOH concentrations, partial pressures, and current densities.

SUPPLEMENTAL INFORMATION

Supplemental Information can be found online at https://doi.org/10.1016/j.joule.2021.01.007.

ACKNOWLEDGMENTS

The authors acknowledge Ontario Centre for the Characterization of Advanced Materials (OCCAM) for sample preparation and characterization facilities. Funding: this work received financial support from the Ontario Research Foundation: Research Excellence Program, the Natural Sciences and Engineering Research Council (NSERC) of Canada, the CIFAR Bio-Inspired Solar Energy program and TOTAL S.E. and the Joint Centre of Artificial Synthesis, a DOE Energy Innovation Hub, supported through the Office of Science of the US Department of Energy under award no. DE-SC0004993. D.S. acknowledges the NSERC E.W.R Steacie Memorial Fellowship. A.T. acknowledges Marie Skłodowska-Curie Fellowship H2020-MSCA-IF-2017 (793471). The authors thank Dr. Y.-F. Liao for the GIWAXS measurements at Spring-8 BL-12B2 beamline of NSRRC. The authors also thank Dr. T. Regier for their assistance at the SGM beamline of CLS.

AUTHOR CONTRIBUTIONS

D.S. and E.H.S. supervised the project. A.O. carried out all the electrochemical experiments with advice from Y.W. and F.L. A.T., A.R.-H., J.C.P., and T.A. designed and synthesized the N-tolylpyridinium molecule and contributed to the manuscript

editing. A.O. and F.L. carried out Raman spectroscopies. Y.W. performed the SEM and TEM analysis. A.O. performed the nuclear magnetic resonance spectroscopies. A.O. and Y.W. co-wrote the manuscript. J.S. performed the TEA modeling. T.B. conducted the CO diffusion modeling. M.L., Y.L., and H.Y. contributed to the discussions and manuscript editing. A.O., Y.W., and F.L. provided equal contributions to this study. All authors contributed to the manuscript.

DECLARATION OF INTERESTS

A.O., Y.W., F.L., D.S., and E.H.S. have filled provisional patent application no. 63/135,277 regarding Cascade CO_2 electroreduction systems.

Received: October 19, 2020
Revised: December 1, 2020
Accepted: January 21, 2021
Published: February 15, 2021

REFERENCES

1. Global data. (2019). Global ethylene industry outlook to 2023 – capacity and capital expenditure forecasts with details of all active and planned plants. https://store.globaldata.com/report/gdch0048icr–global-ethylene-industry-outlook-to-2023-capacity-and-capital-expenditure-forecasts-with-details-of-all-active-and-planned-plants/.

2. Ren, T., Patel, M.K., and Blok, K. (2008). Steam cracking and methane to olefins: energy use, CO2 emissions and production costs. Energy *33*, 817–833.

3. Hepburn, C., Adlen, E., Beddington, J., Carter, E.A., Fuss, S., Mac Dowell, N., Minx, J.C., Smith, P., and Williams, C.K. (2019). The technological and economic prospects for CO2 utilization and removal. Nature *575*, 87–97.

4. Luna, P.D., Hahn, C., Higgins, D., Jaffer, S.A., Jaramillo, T.F., and Sargent, E.H. (2019). What would it take for renewably powered electrosynthesis to displace petrochemical process? Science *364*, eaav3506.

5. Dinh, C.T., Burdyny, T., Kibria, M.G., Seifitokaldani, A., Gabardo, C.M., García de Arquer, F.P., Kiani, A., Edwards, J.P., De Luna, P., Bushuyev, O.S., et al. (2018). CO2 electroreduction to ethylene via hydroxide-mediated copper catalysis at an abrupt interface. Science *360*, 783–787.

6. Li, F., Thevenon, A., Rosas-Hernández, A., Wang, Z., Li, Y., Gabardo, C.M., Ozden, A., Dinh, C.T., Li, J., Wang, Y., et al. (2020). Molecular tuning of CO2-to-ethylene conversion. Nature *577*, 509–513.

7. Wang, Y., Shen, H., Livi, K.J.T., Raciti, D., Zong, H., Gregg, J., Onadeko, M., Wan, Y., Watson, A., and Wang, C. (2019). Copper nanocubes for CO2 reduction in gas diffusion electrodes. Nano Lett. *19*, 8461–8468.

8. Ripatti, D.S., Veltman, T.R., and Kanan, M.W. (2019). Carbon monoxide gas diffusion electrolysis that produces concentrated C2 products with high single-pass conversion. Joule *3*, 240–256.

9. Jouny, M., Hutchings, G.S., and Jiao, F. (2019). Carbon monoxide electroreduction as an emerging platform for carbon utilization. Nat. Catal. *2*, 1062–1070.

10. Liu, Z., Yang, H., Kutz, R., and Masel, R.I. (2018). CO2 electrolysis to CO and O2 at high selectivity, stability and efficiency using sustainion membranes. J. Electrochem. Soc. *165*, J3371–J3377.

11. Gabardo, C.M., O'Brien, C.P., Edwards, J.P., McCallum, C., Xu, Y., Dinh, C.T., Li, J., Sargent, E.H., and Sinton, D. (2019). Continuous carbon dioxide electroreduction to concentrated multi-carbon products using a membrane electrode assembly. Joule *3*, 2777–2791.

12. Wang, L., Higgins, D.C., Ji, Y., Morales-Guio, C.G., Chan, K., Hahn, C., et al. (2020). Selective reduction of CO to acetaldehyde with CuAg electrocatalysts. Proc. Natl. Acad. Sci. U.S.A. *117*, 12572–12575. https://www.pnas.org/content/117/23/12572.short.

13. Skafte, T.L., Blennow, P., Hjelm, J., and Graves, C.R. (2018). Carbon deposition and sulfur poisoning during CO2 electrolysis in nickel-based solid oxide cell electrodes. J. Power Sources *373*, 54–60.

14. Navasa, M., Frandsen, H.L., Skafte, T.L., Sundén, B., and Graves, C. (2018). Localized carbon deposition in solid oxide electrolysis cells studied by multiphysics modeling. J. Power Sources *394*, 102–113.

15. Wang, Y., Wang, Z., Dinh, C.T., Li, J., Ozden, A., Golam Kibria, M.G., Seifitokaldani, A., Tan, C.-S., Gabardo, C.M., Luo, M., et al. (2020). Catalyst synthesis under CO2 electroreduction favours faceting and promotes renewable fuels electrosynthesis. Nat. Catal. *3*, 98–106.

16. Pérez-Gallent, E., Marcandalli, G., Figueiredo, M.C., Calle-Vallejo, F., and Koper, M.T.M. (2017). Structure- and potential-dependent cation effects on CO reduction at copper single-crystal electrodes. J. Am. Chem. Soc. *139*, 16412–16419.

17. Wakerley, D., Lamaison, S., Ozanam, F., Menguy, N., Mercier, D., Marcus, P., Fontecave, M., and Mougel, V. (2019). Bio-inspired hydrophobicity promotes CO2 reduction on a Cu surface. Nat. Mater. *18*, 1222–1227.

18. Schalenbach, M., Hoefner, T., Paciok, P., Carmo, M., Lueke, W., and Stolten, D. (2015). Gas permeation through nafion. Part 1: measurements. J. Phys. Chem. C *119*, 25145–25155.

19. Subbaraman, R., Strmcnik, D., Stamenkovic, V., and Markovic, N.M. (2010). Three phase interfaces at electrified metal−solid electrolyte systems 1. Study of the Pt(hkl)−nafion interface. J. Phys. Chem. C *114*, 8414–8422.

20. García de Arquer, F.P.G.d., Dinh, C.T., Ozden, A., Wicks, J., McCallum, C., Kirmani, A.R., Nam, D.H., Gabardo, C., Seifitokaldani, A., Wang, X., et al. (2020). CO2 electrolysis to multicarbon products at activities greater than 1 A cm-2. Science *367*, 661–666.

21. Jones, D. (2015). Perfluorosulfonic acid membranes for fuel cell and electrolyser applications. Mater. Matters *10*, 42.

22. Han, Z., Kortlever, R., Chen, H.Y., Peters, J.C., and Agapie, T. (2017). CO2 reduction selective for C≥2 products on polycrystalline copper with N-substituted pyridinium additives. ACS Cent. Sci. *3*, 853–859.

23. Gunathunge, C.M., Li, X., Li, J., Hicks, R.P., Ovalle, V.J., and Waegele, M.M. (2017). Spectroscopic observation of reversible surface reconstruction of copper electrodes under CO2 reduction. J. Phys. Chem. C *121*, 12337–12344.

24. Heyes, J., Dunwell, M., and Xu, B. (2016). CO2 reduction on Cu at low overpotentials with surface-enhanced in situ spectroscopy. J. Phys. Chem. C *120*, 17334–17341.

25. Akemann, W., and Otto, A. (1991). Vibrational modes of CO adsorbed on disordered copper films. J. Raman Spectrosc. *22*, 797–803.

26. Pérez-Gallent, E., Figueiredo, M.C., Calle-Vallejo, F., and Koper, M.T.M. (2017). Spectroscopic observation of a hydrogenated CO dimer intermediate during CO reduction

on Cu(100) electrodes. Angew. Chem. Int. Ed. Engl. *129*, 3675–3678.

27. Cheng, T., Xiao, H., and Goddard, W.A., III. (2017). Full atomistic reaction mechanism with kinetics for CO reduction on Cu(100) from ab initio molecular dynamics free-energy calculations at 298 K. Proc. Natl. Acad. Sci. USA *114*, 1795–1800.

28. Gunathunge, C.M., Ovalle, V.J., Li, Y., Janik, M.J., and Waegele, M.M. (2018). Existence of an electrochemically inert CO population on Cu electrodes in alkaline pH. ACS Catal. *8*, 7507–7516.

29. Oda, I., Ogasawara, H., and Ito, M. (1996). Carbon monoxide adsorption on copper and silver electrodes during carbon dioxide electroreduction studied by infrared reflection absorption spectroscopy and surface-enhanced Raman spectroscopy. Langmuir *12*, 1094–1097.

30. Wuttig, A., Liu, C., Peng, Q., Yaguchi, M., Hendon, C.H., Motobayashi, K., Ye, S., Osawa, M., and Surendranath, Y. (2016). Tracking a common surface-bound intermediate during CO2-to-fuels catalysis. ACS Cent. Sci. *2*, 522–528.

31. Liu, X., Schlexer, P., Xiao, J., Ji, Y., Wang, L., Sandberg, R.B., Tang, M., Brown, K.S., Peng, H., Ringe, S., et al. (2019). pH effects on the electrochemical reduction of CO(2) towards C2 products on stepped copper. Nat. Commun. *10*, 32.

32. Jouny, M., Luc, W., and Jiao, F. (2018). High-rate electroreduction of carbon monoxide to multi-carbon products. Nat. Catal. *1*, 748–755.

33. Aeshala, L.M., Uppaluri, R.G., and Verma, A. (2013). Effect of cationic and anionic solid polymer electrolyte on direct electrochemical reduction of gaseous CO2 to fuel. Journal of CO2 Utilization *3* (4), 49–55.

34. Merino-Garcia, I., Albo, J., Solla-Gullón, J., Montiel, V., and Irabien, A. (2019). Cu oxide/ZnO-based surfaces for a selective ethylene production from gas-phase CO2 electroconversion. Journal of CO2 Utilization *31*, 135–142.

35. Merino-Garcia, I., Albo, J., and Irabien, A. (2017). Productivity and selectivity of gas-phase CO2 electroreduction to methane at copper nanoparticle-based electrodes. Energy Technol. *5*, 922–928.

36. Verma, S., Lu, S., and Kenis, P.J.A. (2019). Co-electrolysis of CO2 and glycerol as a pathway to carbon chemicals with improved technoeconomics due to low electricity consumption. Nat. Energy *4*, 466–474.

37. Ge, Q., Hu, Y., Li, B., and Wang, B. (2016). Synthesis of conjugated polycyclic quinoliniums by rhodium(III)-catalyzed multiple C–H activation and annulation of arylpyridiniums with alkynes. Org. Lett. *18*, 2483–2486.

38. Wuttig, A., Yaguchi, M., Motobayashi, K., Osawa, M., and Surendranath, Y. (2016). Inhibited proton transfer enhances Au-catalyzed CO2-to-fuels selectivity. Proc. Natl. Acad. Sci. USA *113*, E4585–E4593.

39. Sheppard, N., and Nguyen, T.T. (1978). Advances in Infrared and Raman Spectroscopy, *5* (Heyden and Sons), pp. 67–148.